

Resonant backward scattering of light by a two-side-open subwavelength metallic slit

S. V. Kukhlevsky^a, M. Mechler^b, L. Csapó^c, K. Janssens^d, O. Samek^e

^a*Institute of Physics, University of Pécs, Ifjúság u. 6, Pécs 7624, Hungary*

^b*South-Trans-Danubian Cooperative Research Centre,
University of Pécs, Ifjúság u. 6, Pécs 7624, Hungary*

^c*Institute of Mathematics and Information, University of Pécs, Ifjúság u. 6, Pécs 7624, Hungary*

^d*Department of Chemistry, University of Antwerp, Universiteitsplein 1, B-2610 Antwerp, Belgium*

^e*Institute of Spectrochemistry and Applied Spectroscopy,
Bunsen-Kirchhoff-Str. 11, D-44139 Dortmund, Germany*

The backward scattering of TM-polarized light by a two-side-open subwavelength slit in a metal film is analyzed. We show that the reflection coefficient versus wavelength possesses a Fabry-Perot-like dependence that is similar to the anomalous behavior of transmission reported in the study [Y. Takakura, Phys. Rev. Lett. **86**, 5601 (2001)]. The open slit totally reflects the light at the near-to-resonance wavelengths. In addition, we show that the interference of incident and resonantly backward-scattered light produces in the near-field diffraction zone a spatially localized wave whose intensity is $10\text{-}10^3$ times greater than the incident wave, but one order of magnitude smaller than the intra-cavity intensity. The amplitude and phase of the resonant wave at the slit entrance and exit are different from that of a Fabry-Perot cavity.

PACS numbers: 78.66.Bz; 42.25.Fx; 07.79.Fc; 42.79.Ag

I. INTRODUCTION

The most impressive features of light scattering by subwavelength metallic nanostructures are resonant enhancement and localization of the light by excitation of electron waves in the metal (for example, see refs. 1,2,3,4,5,6,7,8,9,10,11,12,13,14,15,16,17,18,19,20,21,22,23,24,25,26,27,28,29,30,31,32,33,34,35,36,37,38,39).

In the last few years, a great number of studies have been devoted to the nanostructures in metal films, namely a single aperture, a grating of apertures and an aperture surrounded by grooves. Since the recent paper of Ebbesen and colleagues⁴ on the resonantly enhanced transmission of light observed for a 2D array of subwavelength holes in metal films, the resonant phenomenon is intensively discussed in the literature.^{4,5,6,7,8,9,10,11,12,13,14,15,16,17,18,19,20,21,22,23,24,25,26,27,28,29,30,31,32,33,34,35,36,37,38,39}

Such a kind of light scattering is usually called a Wood's anomaly. In the early researches, Hessel and Oliner showed that the resonances come from coupling between nonhomogeneous diffraction orders and eigenmodes of the grating.⁵ Neviere and co-workers discovered two other possible origins of the resonances.^{6,7} One appears when the surface plasmons of a metallic grating are excited. The other occurs when a metallic grating is covered by a dielectric layer, and corresponds to guided modes resonances in the dielectric film. The role of resonant Wood's anomalies and Fano's profiles in the resonant transmission were explained in the study.⁸

The phenomena involved in propagation through hole arrays are different from those connected with slit arrays. In a slit waveguide there is always a propagating mode inside the channel, while in a hole waveguide all modes are evanescent for hole diameters smaller than approximately a wavelength. In the case of slit apertures in a thick metal film, the transmission exhibits enhancement due to a pure geometrical reason, the resonant excitation of prop-

agating modes inside the slit waveguide.^{9,10,11,12,13} At the resonant wavelengths, the transmitted field increases via the strong coupling of an incident wave with the waveguide modes giving a Fabry-Perot-like behavior.^{10,13,14,15} In the case of films, whose thickness are too small to support the intra-cavity resonance, the extraordinary transmission can be caused by another mechanism, the generation of resonant surface plasmon polaritons and coupling of them into radiation.^{4,9,11,16,22} Both physical mechanisms play important roles in the extraordinary transmission through arrays of two-side-open slits (transmission gratings) and the resonant reflection by arrays of one-side-open slits (reflection gratings). A model of trapped (waveguide) modes has been recently used to show that an array of two-side-open slits can operate like a reflection grating totally reflecting TE-polarized light.¹⁷ The surface plasmons and Rayleigh anomalies were involved in explanation of reflective properties of such a kind of gratings.¹⁸

The studies^{13,14,15,19} have pointed out that the origin of anomalous scattering of light by a grating of slits (holes) can be better understood by clarifying the transmission and reflection properties of a single subwavelength slit. Along this direction, it was already demonstrated that the intensity of TM-polarized light resonantly transmitted through a single slit can be $10\text{-}10^3$ times higher than the incident wave^{1,2,3,15} and that the transmission coefficient versus wavelength possesses a Fabry-Perot-like behavior^{13,14,15}. Unfortunately, the reflection properties of the slit have received no attention in the literature. The very recent study¹⁷ only concerned the problem by regarding the total reflection of TE-polarized light by a grating of two-side-open slits to properties of the independent slit emitters.

In this article, the backward scattering of light by a two-side-open subwavelength slit is analyzed. To com-

pare properties of the light reflection with the extraordinary transmission^{13,14,15}, we consider the scattering of TM-polarized light by a slit in a thick metallic film of perfect conductivity. From the latter metal property it follows that surface plasmons do not exist in the film. Such a metal can be described by the Drude model for which the plasmon frequency tends towards infinity. The traditional approach based on the Neerhoff and Mur solution of Maxwell's equations is used in the computations.^{1,2,3} The article is organized as follows. The theoretical background, numerical analysis and discussion are presented in Section II. The summary and conclusions are given in Section III. The brief description of the model is presented in the Appendix.

II. NUMERICAL ANALYSIS AND DISCUSSION

It is well known that when a light wave is scattered by a subwavelength metallic object, a significant part of the incident light can be scattered backward (reflected) whatever the object be reflecting or transparent. It was recently demonstrated that an array of two-side-open subwavelength metallic slits effectively reflects light waves at the appropriate resonant conditions.^{17,18} One may suppose that this is true also in the case of a single slit. In this section, we test whether a light wave can be resonantly reflected by a single two-side-open subwavelength metallic slit. To address this question, the energy flux in front of the slit is analyzed numerically for various regimes of the light scattering. In order to compare properties of the light reflection with that of the extraordinary (resonant) transmission^{13,14,15}, we consider the zeroth-order scattering of a time-harmonic wave of TM-polarized light by a slit in a perfectly conducting thick metal film placed in vacuum (Fig. 1). The energy flux \vec{S}_I in front of the slit is compared with the fluxes \vec{S}_{II} and \vec{S}_{III} inside the slit and behind the slit, respectively. The amplitude and phase of the light wave at the slit entrance and exit are compared with that of a Fabry-Perot cavity. The electric \vec{E} and magnetic \vec{H} fields of the light are computed by using the traditional approach based on the Neerhoff and Mur solution of Maxwell's equations.^{1,2,3} For more details of the model, see the Appendix.

According to the model, the electric $\vec{E}(x, z)$ and magnetic $\vec{H}(x, z)$ fields in front of the slit (region I), inside the slit (region II) and behind the slit (region III) are determined by the scalar fields $U_1(x, z)$, $U_2(x, z)$ and $U_3(x, z)$, respectively. The scalar fields are found by solving the Neerhoff and Mur integral equations. The magnetic field of the wave is assumed to be time harmonic and constant in the y direction: $\vec{H}(x, y, z, t) = U(x, z) \exp(-i\omega t) \vec{e}_y$. In front of the slit, the field is decomposed into $U_1(x, z) = U^i(x, z) + U^r(x, z) + U^d(x, z)$. The field $U^i(x, z)$ represents the incident field, which is assumed to be a plane wave of unit amplitude; $U^r(x, z)$ denotes the field that would be reflected if there were no slit in the film;

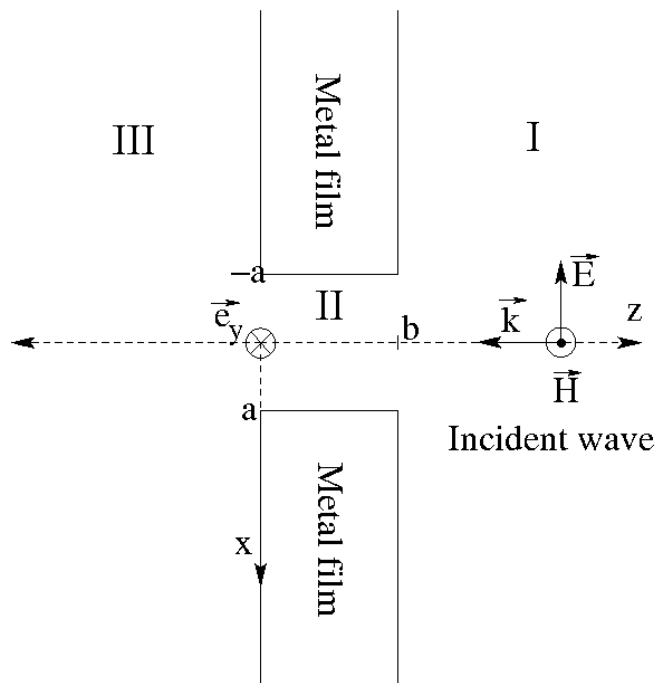
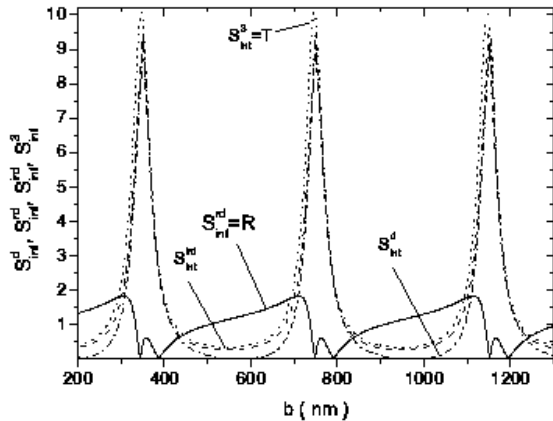


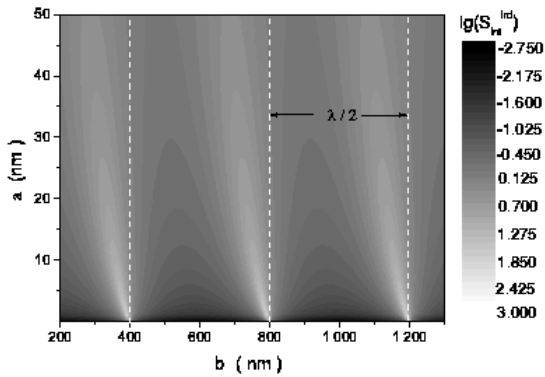
FIG. 1: Propagation of a continuous wave through a subwavelength nano-sized slit in a thick metal film.

$U^d(x, z)$ describes the backward diffracted field due to the presence of the slit. The time averaged Poynting vector (energy flux) \vec{S} of the electromagnetic field is calculated (in CGS units) as $\vec{S} = (c/16\pi)(\vec{E} \times \vec{H}^* + \vec{E}^* \times \vec{H})$. The reflection coefficient $R = S_{int}^{rd}$ is given by the normalized flux $S_n^{rd} = S^{rd}/S^i$ integrated over the slit width $2a$ at the slit entrance ($z = b$), where S^{rd} is the z component of the backward scattered flux, and S^i is the incident flux along the z direction. The flux $S^{rd} = S^{rd}(U^r, U^d)$ is produced by the interference of the backward scattered fields $U^r(x, z)$ and $U^d(x, z)$. The transmission coefficient $T = S_{int}^3(b)$ is determined by the normalized flux $S_n^3 = S^3/S^i$ integrated over the slit width at the slit exit ($z = 0$), where the flux z -component $S^3 = S^3(U^3)$ is produced by the forward scattered (transmitted) field $U^3(x, z)$. Notice that the definitions of the reflection R and transmission T coefficients are equivalent to the more convenient ones defined as the integrated reflected or transmitted flux divided by the integrated incident flux. In the following analysis, the reflection and transmission coefficients are compared to the fluxes S_{int}^d and S_{int}^{ird} obtained by integrating the normalized fluxes $S_n^d = S^d/S^i$ and $S_n^{ird} = S^{ird}/S^i$, respectively.

We analyzed the backward scattering of light for a wide range of scattering conditions determined by values of the wavelength λ , slit width $2a$ and film thickness b . As an example, the reflection coefficient $R = S_{int}^{rd}(b)$ as a function of the film thickness b computed for the wavelength $\lambda = 800$ nm and the slit width $2a = 25$ nm is shown in Fig. 2(a). The transmission coefficient $T = S_{int}^3(b)$ and



(a)



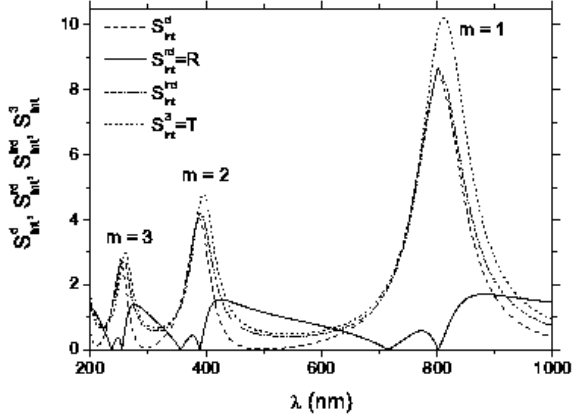
(b)

FIG. 2: (a) The reflection coefficient $R = S_{int}^{rd}(b)$, the transmission coefficient $T = S_{int}^3(b)$, and the integrated fluxes $S_{int}^d(b)$ and $S_{int}^{ird}(b)$ as a function of the film thickness b computed for the wavelength $\lambda = 800$ nm and the slit width $2a = 25$ nm. (b) The logarithm of the integrated flux $S_{int}^{ird}(a, b)$ as a function of the slit half-width a and film thickness b .

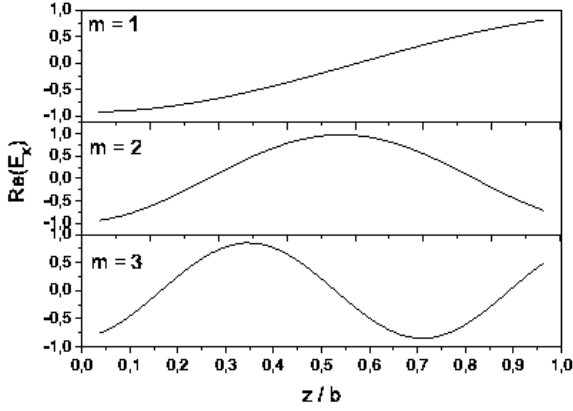
the integrated fluxes $S_{int}^d(b)$ and $S_{int}^{ird}(b)$ are presented in the figure for the comparison. We note the reflection resonances of $\lambda/2$ periodicity with the maxima $R_{max} \approx 2$. In agreement with the previous results^{13,14,15}, one can see also the transmission resonances having the same period, and the peak heights $T \approx 10$ ($T \approx \lambda/2\pi a$) at the resonances. It is worth to note the correlation between the positions of maxima and minima in the reflection and transmission. The resonance positions for the total reflection are somewhat left-shifted with respect to the transmission resonances. The maxima of the transmission

efficient correspond to reflection minima. In Fig. 2(a), one can observe also many satellite peaks in reflection. For one broad minimum, it appears a local reflection maximum, which is characterized by a weak amplitude. The local maxima appear before 400, 800, and 1200 nm. The positions of the local maxima approximately correspond to the S_{int}^d maxima. To clarify a role of the fields U^i , U^r , U^d and U^3 in the resonant backward scattering, we compared the integrated flux $S_{int}^{ird}(U^i, U^r, U^d)$ with the fluxes $S_{int}^d(U^d)$ and $S_{int}^3(U^3) = T$. One can see from Fig. 2(a) that the flux S_{int}^{ird} produced in front of the slit by the interference of the incident field $U^i(x, z)$ and the backward scattered fields $U^r(x, z)$ and $U^d(x, z)$ is practically undistinguishable from that generated by the backward diffracted field U^d and forward scattered (transmitted) field U^3 . The integrated flux $S_{int}^{ird}(a, b)$ as a function of the slit half-width a and film thickness b is shown in Fig. 2(b). We notice that the widths and shifts of the resonances increase with increasing the value a . Analysis of Fig. 2(a) indicates that the difference between the integrated fluxes $S_{int}^{rd}(U^r, U^d) = R$ and $S_{int}^3(U^3) = T$ ($T \approx S_{int}^d(U^d)$) appears due to the interference of the backward diffracted field $U^d(x, z)$ and the reflected field $U^r(x, z)$.

The dispersion of the reflection coefficient $R(\lambda) = S_{int}^{rd}(\lambda)$ for the slit width $2a = 25$ nm and the screen thickness $b = 351$ nm is shown in Fig. 3(a). The integrated fluxes $S_{int}^d(\lambda)$, $S_{int}^{ird}(\lambda)$ and $S_{int}^3(\lambda) = T(\lambda)$ versus the wavelength are shown in the figure for the comparison. A very interesting behavior of the dispersion is that the coefficient R versus the wavelength λ possesses a Fabry-Perot-like dependence that is similar to the anomalous behavior of transmission $T(\lambda)$ reported in the studies^{10,13,14,15,19}. In agreement with the studies^{1,2,3,15}, the height of the first (maximum) transmission peak is given by $T \approx \lambda_r^1/2\pi a$. The wavelengths corresponding to the resonant peaks $\lambda_r^m \approx 2b/m$ ($m = 1, 2, 3, \dots$) are in accordance with the results¹³. The high peak amplitudes (enhancement), however, are different from the low magnitudes (attenuation) predicted in the study¹³, but compare well with the experimental and theoretical results^{1,2,3,14,15}. The difference is caused by the manner in which the Maxwell equations are solved. The study¹³ uses a simplified approach based on the matching the cavity modes expansion of the light wave inside the slit with the plain waves expansion above and below the slit using two boundary conditions, at $z = 0$ and $|z| = b$. Conversely, the Neerhoff and Mur method performs the matching with five boundary conditions, at $z \rightarrow 0$, $z \rightarrow b$, $x \rightarrow a$, $x \rightarrow -a$, and $r \rightarrow \infty$. In contrast to the sharp Lorentzian-like transmission peaks, the slit forms very wide Fano-type reflection bands (see, Fig. 3(a)). For one broad minimum in reflection, it appears also a local reflection maximum, which is characterized by weak amplitude. At the near-to-resonance wavelengths of the transmission, the open aperture totally reflects the light. It is worth to note the correlation between the wavelengths for maxima and minima in the reflection $R(\lambda)$, transmission



(a)



(b)

FIG. 3: (a) The reflection coefficient $R = S_{int}^d(\lambda)$, the transmission coefficient $T = S_{int}^3(\lambda)$, and the integrated fluxes $S_{int}^d(\lambda)$ and $S_{int}^3(\lambda)$ versus the wavelength λ computed for the slit width $2a = 25$ nm and the screen thickness $b = 351$ nm. (b) The real part of the normalized electric field x-component $E_x(U_2) = E_x(x, z)$ versus the normalized distance z/b inside the slit cavity at $x = 0$, for the resonant wavelength $\lambda_r^1 = 800$ nm, $\lambda_r^2 = 389$ nm, $\lambda_r^3 = 255$ nm.

$T(\lambda)$, and the flux S_{int}^d (Table I). The resonance wavelengths for the main reflection maxima are red-shifted with respect to the transmission resonances. The wavelengths of both the transmission and reflection (main and little) resonances are red-shifted with respect to the Fabry-Perot wavelengths $\lambda_r^m = 702$ nm, 351 nm, ... ($\lambda_r^m \approx 2b/m$, $m = 1, 2, 3, \dots$). To understand the physical mechanism of the resonant backward scattering, we also compared the integrated flux $S_{int}^{ird}(U^i, U^r, U^d)$ with the fluxes $S_{int}^d(U^d)$ and $S_{int}^3(U^3) = T$. As can

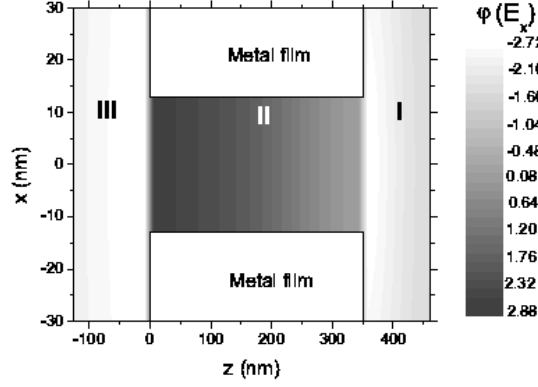
λ (nm) of	R_{max}^{main}	R_{max}^{little}	R_{min}
	276	248	237
	426	377	255
	882	773	356
			389
			714
			802

λ (nm) of	T_{max}	T_{min}	S_{max}^d
	260	226	253
	396	315	388
	812	542	802

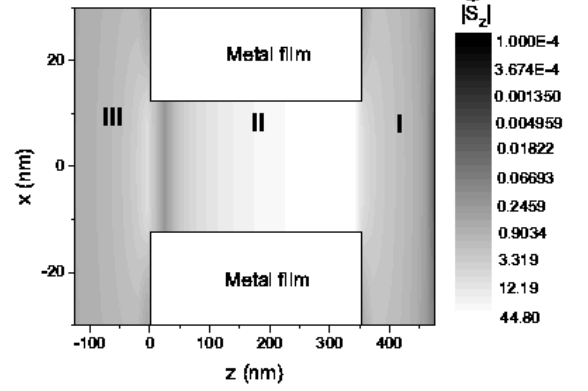
TABLE I: The wavelengths for maxima and minima in the reflection $R(\lambda)$, transmission $T(\lambda)$, and the flux S_{int}^d .

be seen from Fig. 3(a), the integrated fluxes $S_{int}^d(\lambda)$, $S_{int}^{ird}(\lambda)$ and $S_{int}^3(\lambda) = T(\lambda)$ are practically undistinguishable also in the λ -domain (for the b -domain, see Fig. 2(a)). The difference between the integrated fluxes $S_{int}^{rd}(U^r, U^d) = R$ and $S_{int}^3(U^3) = T$ ($T \approx S_{int}^d(U^d)$) is caused by the interference of the backward diffracted field $U^d(x, z)$ and the reflected field $U^r(x, z)$ in the energy flux $\vec{S} \sim (\vec{E} \times \vec{H}^* + \vec{E}^* \times \vec{H})$. The wavelengths of the little maxima of the reflection $R = R(U^d, U^r)$ correspond approximately to the high maxima S_{int}^d . Therefore, the little maxima can be attributed to the interference of the reflected field U^r with the dominant diffracted field U^d . The red shifts and the asymmetrical shapes of the reflection bands can be explained by a Fano analysis⁸ of the scattering problem by distinguishing resonant and non-resonant interfering contributions to the reflection process. The resonant contribution is given by the field U^d and the non-resonant one is attributed to the field U^r . Other interesting interpretations of the shifts of resonant wavelengths in the transmission spectra from the values $2b/m$ can be found in the studies^{10,13,14,15,17,23}. It should be mentioned that the asymmetrical behavior of reflection was observed also in the case of a Fabry-Perot resonator^{24,25}. The conditions to achieve such an asymmetry are rested on the existence of dissipative loss in the resonator. There is no explicit loss in the present problem, but the dissipative loss can be substituted by radiative loss due to the diffraction by the slit.

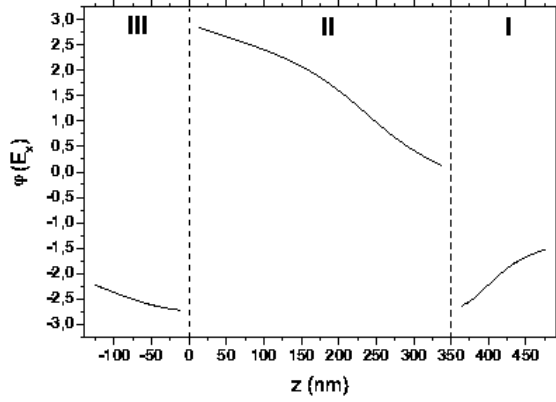
After the analysis of Fig. 2(a), it is not surprising that the maxima of the transmission are accompanied by the minima of the reflection also in the λ -domain (see, Fig. 3(a)). It should be noted in this connection that such a behavior of $R(\lambda)$ and $T(\lambda)$ is similar to that observed in the case of excitation of the surface plasmons in an array of slit in a thin metal film.¹⁸ In the study¹⁸, the minima in reflection spectra corresponding to the maxima in the transmission spectra were attributed to the redistribution of the energy of diffracted evanescent order into the propagating order. In the case of a thick film, we explain such a behavior by another physical mechanism, the interference of the backward diffracted field $U^d(x, z)$ and the reflected field $U^r(x, z)$. It can be noted that the corre-



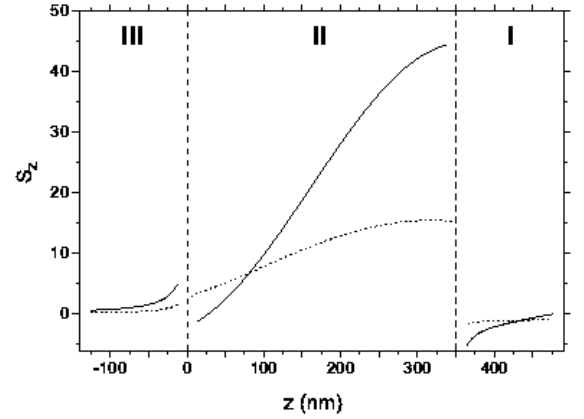
(a)



(a)



(b)



(b)

FIG. 4: (a) The phase distribution $\varphi(x, z)$ of the electric field x -component $E_x(x, z)$ inside and outside the slit. The field component $E_x(x, z)$ is given by $E_x(U^i, U^r, U^d)$, $E_x(U^2)$ and $E_x(U^3)$ in the regions I, II and III, respectively. (b) The phase distribution $\varphi(x, z)$ at $x = 0$. The slit width $2a = 25$ nm, the film thickness $b = 351$ nm and the wavelengths $\lambda = 800$ nm.

lation of positions of reflection minima and transmission maxima (see, Figs. 2(a) and 3(a)) are consistent with that predicted by the study¹⁷ for TE-polarized light scattered by a grating of two-side-open slits in a thick metal film. However, the values of $R(\lambda)$ and $T(\lambda)$ are in contrast to the relation $R(\lambda) + T(\lambda) = 1$ given in the study¹⁷. The difference can be explained by the fact that we examined light scattering by an infinite screen using local definitions of R and T , while the study¹⁷ analyzed the global reflection and transmission by a grating of finite size.

The dispersions $S_{int}^d(\lambda)$, $S_{int}^{ird}(\lambda)$ and $S_{int}^3(\lambda) = T(\lambda)$ shown in Fig. 3(a) indicate the wave-cavity interaction behavior, which is similar to that in the case of a Fabry-

FIG. 5: (a) The spatial distribution $|\vec{S}_z(x, z)|$ of the absolute value of the normalized energy flux along the z direction inside and outside the slit. The distribution $|S_z(x, z)|$ is shown in the logarithmical scale. The flux S_z is given by the normalized fluxes $S^{ird}(U^i, U^r, U^d)/S^i(U^i)$, $S^2(U^2)/S^i(U^i)$ and $S^3(U^3)/S^i(U^i)$ for the regions I, II and III, respectively. (b) The energy flux distribution $S_z(x, z)$ at $x = 0$. The slit width $2a = 25$ nm, the film thickness $b = 351$ nm and the wavelength $\lambda = 800$ nm (solid line) and $\lambda = 882$ nm (dotted line) corresponding to a transmission resonance and a little reflection resonance, respectively.

Perot resonator. The fluxes $S_{int}^d(U^d)$, $S_{int}^{ird}(U^i, U^r, U^d)$ and $S_{int}^3(U^3) = T$ exhibit the Fabry-Perot-like maxima around the resonance wavelengths $\lambda_r^m \approx 2b/m$. In order to understand the connection between the Fabry-Perot-like resonances and the total reflection, we computed the amplitude and phase distributions of the light wave at the resonant and near-resonant wavelengths in-

side and outside the slit cavity (see, Figs. 3(b), 4 and 5). At the resonance wavelengths, the intra-slit fields possess maximum amplitudes with Fabry-Perot-like spatial distributions (Fig. 3(b)). However, in contrast to the Fabry-Perot-like modal distributions, the resonant configurations are characterized by antinodes of the electric field at each open aperture of the slit. Such a behavior is in agreement with the results^{10,20,21}. It is interesting that at the slit entrance, the amplitudes E_x of the resonant field configuration possesses the Fabry-Perot-like phase shift on the value of π (Fig. 4). The integrated fluxes $S_{int}^{ird}(U^i, U^r, U^d)$, $S_{int}^d(U^d)$ and $S_{int}^3(U^3)$, at the first resonant wavelength λ_r^1 , exhibit enhancement by a factor $\lambda/2\pi a \approx 10$ with respect to the incident wave (Fig. 3(a)). For the comparison, the normalized resonant fluxes $S_n^{ird}(U^i, U^r, U^d)$ and $S_n^3(U^3)$ in the near-field zone ($z \approx -2a$) are about 5 times greater than the incident wave (see, Fig. 5). It should be stressed that the resonantly enhanced intra-cavity intensity $S_n^2(U^2)$ is about 10 times higher than the resonant fluxes $S_n^{ird}(U^i, U^r, U^d)$ and $S_n^3(U^3)$ localized in the near field zone in front of the slit and behind the slit, respectively (Fig. 5). The interference of the incident $U^i(x, z)$ wave and the backward scattered fields $U^r(x, z)$ and $U^d(x, z)$, at the resonant wavelengths $\lambda_r^m \approx 2b/m$, produces in the near-field diffraction zone a strongly localized wave whose normalized flux $S_n^{ird}(U^i, U^r, U^d)$ is $\lambda/2\pi a \approx 10 \cdot 10^3$ times greater than the incident wave, but about one order of magnitude smaller than the resonant intra-cavity intensity.

In our model we considered an incident wave with TM polarization. According to the theory of waveguides, the vectorial wave equations for this polarization can be reduced to one scalar equation describing the magnetic field H of TM modes. The electric component E of these modes is found using the field H and Maxwell's equations. The TM scalar equation for the component H is decoupled from the similar scalar equation describing the field E of TE (transverse electric) modes. Hence, the formalism works analogously for TE polarization exchanging the E and H fields.

III. SUMMARY AND CONCLUSION

In the present paper, the backward scattering of TM-polarized light by a two-side-open subwavelength slit in a metal film has been analyzed. We predict that the reflection coefficient versus wavelength possesses a Fabry-Perot-like dependence that is similar to the anomalous behavior of transmission. The open slit totally reflects the light at the near-to-resonance wavelengths. The resonance wavelengths for the total reflection are somewhat red-shifted with respect to the transmission resonances. The wavelengths of both the reflection and transmission resonances are red-shifted with respect to the Fabry-Perot wavelengths. The sharp resonant maxima of transmission are accompanied by the wide minima of the reflection. In addition, we showed that the in-

terference of incident and resonantly backward-scattered light produces in the near-field diffraction zone a strongly localized wave whose intensity is greater than the incident wave by a factor $\lambda/2\pi a \approx 10 \cdot 10^3$ and about one order of magnitude smaller than the intra-cavity intensity. The correlation between the amplitude and phase distributions of light waves inside and outside the slit was also investigated. The slit cavity was compared with a Fabry-Perot resonator. We showed that the amplitude and phase of the resonant wave at the slit entrance and exit are different from that of a Fabry-Perot cavity. The physical mechanism responsible for the total reflection is the interference of the backward diffracted resonant field $U^d(x, z)$ and the reflected non-resonant field $U^r(x, z)$ in the energy flux at the near-to-resonance wavelengths (Fano-type effect). The wavelength-selective total reflection of light by two-side-open metal slits may find application in many kinds of sensors and actuators. The $(10 \cdot 10^3)$ -times and $(10^2 \cdot 10^4)$ -times enhancement of the light intensity in front of the slit and inside the slit can be used in reflective nanooptics and in intra-cavity spectroscopy of single atoms. We believe that the presented results gain insight into the physics of resonant scattering of light by subwavelength nano-slits in metal films.

Acknowledgments

The authors appreciate the valuable comments and suggestions of the anonymous referees. This study was supported by the Fifth Framework of the European Commission (Financial support from the EC for shared-cost RTD actions: research and technological development projects, demonstration projects and combined projects. Contract NG6RD-CT-2001-00602) and in part by the Hungarian Scientific Research Foundation (OTKA, Contracts T046811 and M045644) and the Hungarian R&D Office (KPI, Contract GVOP-3.2.1.-2004-04-0166/3.0).

Appendix

We briefly describe the Neerhoff and Mur model^{1,3} of the scattering of a plane continuous wave by a subwavelength slit of width $2a$ in a perfectly conducting metal screen of thickness b . The slit is illuminated by a normally incident plane wave under TM polarization (magnetic-field vector parallel to the slit), as shown in Fig. 1. The magnetic field of the wave is assumed to be time harmonic and constant in the y direction:

$$\vec{H}(x, y, z, t) = U(x, z)e^{-i\omega t}\vec{e}_y. \quad (1)$$

The electric field of the wave is found from the scalar field $U(x, z)$ using Maxwell's equations. The restrictions in Eq. (1) reduce the diffraction problem to one involving a single scalar field $U(x, z)$ in two dimensions. The field

is represented by $U_j(x, z)$ ($j=1,2,3$ in region I, II and III, respectively), and satisfies the Helmholtz equation: $(\nabla^2 + k_j^2)U_j = 0$, where $j = 1, 2, 3$. In region I, the field $U_1(x, z)$ is decomposed into three components:

$$U_1(x, z) = U^i(x, z) + U^r(x, z) + U^d(x, z), \quad (2)$$

each of which satisfies the Helmholtz equation. U^i represents the incident field:

$$U^i(x, z) = e^{-ik_1 z}. \quad (3)$$

U^r denotes the reflected field without a slit:

$$U^r(x, z) = U^i(x, 2b - z). \quad (4)$$

Finally, U^d describes the diffracted field in region I due to the presence of the slit. With the above set of equations and standard boundary conditions for a perfectly conducting screen, a unique solution exists for the scattering problem. The solution is found by using the Green function formalism.

The magnetic $\vec{H}(x, z, t)$ fields in regions I, II, and III are given by

$$H^1(x, z) = \exp(-ik_1 z) + \exp(-ik_1(2b - z)) + \frac{ia}{N} \frac{\epsilon_1}{\epsilon_2} \sum_{j=1}^N H_0^1(k_1 \sqrt{(x - x_j)^2 + (z - b)^2}) (DU_b)_j, \quad (5)$$

$$\begin{aligned} H^2(x, z) = & -\frac{i}{2N\sqrt{k_2^2}} e^{i\sqrt{k_2^2}|z|} \sum_{j=1}^N (DU_0)_j + \frac{i}{2N\sqrt{k_2^2}} \\ & \times e^{i\sqrt{k_2^2}|z-b|} \sum_{j=1}^N (DU_b)_j - \frac{1}{2N} e^{i\sqrt{k_2^2}|z|} \sum_{j=1}^N (U_0)_j + \frac{1}{2N} \\ & \times e^{i\sqrt{k_2^2}|z-b|} \sum_{j=1}^N (U_b)_j - \frac{i}{N} \sum_{m=1}^{\infty} \frac{1}{\gamma_1} \cos \frac{m\pi(x+a)}{2a} e^{i\gamma_1|z|} \\ & \times \sum_{j=1}^N \cos \frac{m\pi(x_j+a)}{2a} (DU_0)_j - \frac{1}{N} \sum_{m=1}^{\infty} \cos \frac{m\pi(x+a)}{2a} \\ & \times e^{i\gamma_1|z|} \sum_{j=1}^N \cos \frac{m\pi(x_j+a)}{2a} (U_0)_j + \frac{i}{N} \sum_{m=1}^{\infty} \frac{1}{\gamma_1} e^{i\gamma_1|z-b|} \\ & \times \cos \frac{m\pi(x+a)}{2a} \sum_{j=1}^N \cos \frac{m\pi(x_j+a)}{2a} (DU_b)_j \\ & + \frac{1}{N} \sum_{m=1}^{\infty} \cos(m\pi \frac{x+a}{2a}) e^{i\gamma_1|z-b|} \\ & \times \sum_{j=1}^N \cos \frac{m\pi(x_j+a)}{2a} (U_b)_j, \quad (6) \end{aligned}$$

$$H^3(x, z) = i\epsilon_3 \sum_{j=1}^N \frac{a}{N\epsilon_2} (D\vec{U}_0)_j \times H_0^{(1)} \left[k_3 \sqrt{(x - x_j)^2 + z^2} \right], \quad (7)$$

where $x_j = 2a(j - 1/2)/N - a$, $j = 1, 2, \dots, N$; $N > 2a/z$; $H_0^{(1)}(X)$ is the Hankel function; $\vec{H}^i = H^i \cdot \vec{e}_y$, $i = 1, 2, 3$; $\gamma_m = [k_2^2 - (m\pi/2a)^2]^{1/2}$. The coefficients $(D\vec{U}_0)_j$ are found by solving numerically four coupled integral equations. For more details on the model and the numerical solution of the Neerhoff and Mur coupled integral equations, see the references^{1,3}.

¹ F. L. Neerhoff and G. Mur, Appl. Sci. Res. **28**, 73 (1973).

² R.F. Harrington and D.T. Auckland, IEEE Trans. Anten-

- nas Propag **AP28**, 616 (1980).
- ³ E. Betzig, A. Harootunian, A. Lewis, and M. Isaacson, *Appl. Opt.* **25**, 1890 (1986).
 - ⁴ T.W. Ebbesen, H.J. Lezec, H.F. Ghaemi, T. Thio, and P.A. Wolff, *Nature (London)* **391**, 667 (1998).
 - ⁵ A. Hessel and A.A. Oliner, *Appl. Opt.* **4**, 1275 (1965).
 - ⁶ M. Nevière, D. Maystre, and P. Vincent, *J. Opt.* **8**, 231 (1977).
 - ⁷ D. Maystre and M. Nevière, *J. Opt.* **8**, 165 (1977).
 - ⁸ M. Sarrazin, J.P. Vigneron, and J.M. Vigoureux, *Phys. Rev. B* **67**, 085415 (2003).
 - ⁹ J. A. Porto, F.J. García-Vidal, and J.B. Pendry, *Phys. Rev. Lett.* **83**, 2845 (1999).
 - ¹⁰ S. Astilean, Ph. Lalanne, and M. Palamaru, *Opt. Commun.* **175**, 265 (2000).
 - ¹¹ A.P. Hibbins, J.R. Sambles and C.R. Lawrence, *Appl. Phys. Lett.* **81**, 4661 (2002).
 - ¹² Q. Cao and P. Lalanne, *Phys. Rev. Lett.* **88**, 057403 (2002).
 - ¹³ Y. Takakura, *Phys. Rev. Lett.* **86**, 5601 (2001).
 - ¹⁴ F.Z. Yang and J.R. Sambles, *Phys. Rev. Lett.* **89**, 063901 (2002).
 - ¹⁵ S.V. Kulklevsky, M. Mechler, L. Csapo, K. Janssens, and O. Samek, *Phys. Rev. B* **70**, 195428 (2004).
 - ¹⁶ F.J. García-Vidal, H.J. Lezec, T.W. Ebbesen, and L. Martín-Moreno, *Phys. Rev. Lett.* **90**, 231901 (2003).
 - ¹⁷ A.G. Borisov, F.G. García de Abajo, and S.V. Shabanov, *Phys. Rev. B* **71**, 075408 (2005).
 - ¹⁸ J.M. Steele, C.E. Moran, A. Lee, C.M. Aguirre, and N.J. Halas, *Phys. Rev. B* **68**, 205103 (2003).
 - ¹⁹ F.J. García-Vidal and L. Martín-Moreno, *Phys. Rev. B* **66**, 155412 (2002).
 - ²⁰ J. Lindberg, K. Lindfors, T. Setälä, M. Kaivola, and A.T. Friberg, *Opt. Express* **12**, 623 (2004).
 - ²¹ Y. Xie, A.R. Zakharian, J.V. Moloney, and M. Mansuripur, *Opt. Express* **12**, 6106 (2004).
 - ²² U. Schröter and D. Heitmann, *Phys. Rev. B* **58**, 15419 (1998).
 - ²³ M.M.J. Treacy, *Phys. Rev. Lett.* **75**, 606 (1999).
 - ²⁴ J.M. Vigoureux and R. Giust, *Opt. Commun.* **186**, 21 (2000).
 - ²⁵ J.J. Monzón, T. Yonte, and L.L. Sánchez-Soto, *Opt. Commun.* **218**, 43 (2003).
 - ²⁶ E. Popov, M. Nevière, S. Enoch, and R. Reinisch, *Phys. Rev. B* **62**, 16100 (2000).
 - ²⁷ S.I. Bozhevolnyi, J. Erland, K. Leosson, P.M.W. Skovgaard, and J.M. Hvam, *Phys. Rev. Lett.* **86**, 3008 (2001).
 - ²⁸ A. Barbara, P. Quemerais, E. Bustarret, and T. Lopez-Rios, *Phys. Rev. B* **66**, 161403 (2002).
 - ²⁹ A.M. Dykhne, A.K. Sarychev, and V.M. Shalaev, *Phys. Rev. B* **67**, 195402 (2003).
 - ³⁰ X.L. Shi, L. Hesselink, and R.L. Thornton, *Opt. Lett.* **28**, 1320 (2003).
 - ³¹ H.F. Schouten, T.D. Visser, D. Lenstra, and H. Blok, *Phys. Rev. E* **67**, 036608 (2003).
 - ³² A. Nahata, R.A. Linke, T. Ishi, and K. Ohashi, *Opt. Lett.* **28**, 423 (2003).
 - ³³ A. Bouhelier, M. Beversluis, A. Hartschuh, and L. Novotny, *Phys. Rev. Lett.* **90**, 013903 (2003).
 - ³⁴ K.R. Li, M.I. Stockman, and D.J. Bergman, *Phys. Rev. Lett.* **91**, 227402 (2003).
 - ³⁵ A. Dechant and A.Y. Elezzabi, *Appl. Phys. Lett.* **84**, 4678 (2004).
 - ³⁶ W.J. Fan, S. Zhang, B. Minhas, K.J. Malloy, and S.R.J. Brueck, *Phys. Rev. Lett.* **94**, 033902 (2005).
 - ³⁷ A.V. Zayats, I.I. Smolyaninov, and A.A. Maradudin, *Phys. Rep.* **408**, 131 (2005).
 - ³⁸ M. Labardi, M. Zavelani-Rossi, D. Polli, G. Cerullo, M. Allegrini, S. De Silvestri, and O. Svelto, *Appl. Phys. Lett.* **86**, 031105 (2005).
 - ³⁹ Y. Ben-Aryeh, *International J. Quantum Information* **3**, 111 (2005).